N-Electron Ground State Energies of a Quantum Dot in Magnetic Field

R. C. Ashoori,* H. L. Stormer, J. S. Weiner, L. N. Pfeiffer, K. W. Baldwin, and K. W. West
AT&T Bell Laboratories, Murray Hill, New Jersey 07974
(Received 8 December 1992)

Using single-electron capacitance spectroscopy, we map the magnetic field dependence of the ground state energies of a single quantum dot containing from 0 to 50 electrons. The experimental spectra reproduce many features of a noninteracting electron model with an added fixed charging energy. However, in detailed observations deviations are apparent: Exchange induces a two-electron singlet-triplet transition, self-consistency of the confinement potential causes the dot to assume a quasi-two-dimensional character, and features develop which are suggestive of the fractional quantum Hall effect.

PACS numbers: 73.20.Dx, 71.50.+t, 72.20.My, 73.40.Gk

For a given atomic species, isolated atoms have identical spectra; this property has facilitated the study of atomic physics, as signal levels in experiments can be enhanced by simply creating samples containing many atoms. In contrast, the study of artificially structured atoms in semiconductors, or "quantum dots," has been impeded by nonuniformity in systems of many dots. Recently, two techniques have been developed which allow spectroscopic study of the ground state (g.s.) energies in *individual* quantum dots with a resolution limited only by the temperature of the electronic system [1,2].

A key question to be answered by spectroscopic studies on quantum dots is the role of the electron-electron interaction in modifying the dot's electronic level structure. Bryant [3] has addressed this question for quantum dots containing just two electrons. He finds a continuous evolution of the level structure, from single-particle-like states in the limit of a very small dot, to a level structure dominated by the electron-electron interaction in larger dots. Since the confinement potential in semiconductor quantum dots can be controlled at will, a large range of this continuum which is not accessible in atomic physics can be examined.

In a previous paper [1], we have introduced single-electron capacitance spectroscopy (SECS). The method allows the direct measurement of the energies of quantum levels of an individual small structure (dot) as a function of magnetic field (B). When the Fermi energy of an electrode becomes resonant with a quantum level of a nearby dot, single electrons can tunnel back and forth between the electrode and the dot through a tunnel barrier [see Fig. 1(a)]. The resulting charge induced by this motion on the opposite electrode of a "tunnel capacitor" is detected by an on-chip, highly sensitive transistor. Using this technique we were able to detect spatially distinct localized states in a small tunnel capacitor. In this Letter, we now use SECS to measure the g.s. energies of a single quantum dot containing N electrons in which charge nucleates in only one central location.

The basic configuration of our GaAs samples has been described previously [1], although the semiconductor structure has been slightly modified for the present experiments. A schematic of the sample is shown in Fig. 1(a). The layer sequence is as follows: a 3000 Å n^+-doped (4×10^{17} cm^{-3}) GaAs bottom electrode; a 600 Å undoped GaAs spacer layer; a 125 Å undoped $Al_{0.3}Ga_{0.7}As$/GaAs superlattice tunnel barrier; a 175 Å quantum well (vertically confines the quantum dot); a 500 Å $Al_{0.3}Ga_{0.7}As$ blocking barrier; and a 300 Å GaAs cap layer. The blocking barrier contains a Si delta doped layer 200 Å from the well edge. The wide 600 Å spacer layer and the superlattice tunnel barrier [4] were implemented to prevent Si atoms from migrating into the well [1]. Lateral confinement is provided by first patterning a 3500 Å diam circular metallic disk on top of the sample surface and using this as an etch mask to etch down to the AlGaAs blocking barrier surface. The 3500 Å diam top electrode is contacted for measurement by overlaying it

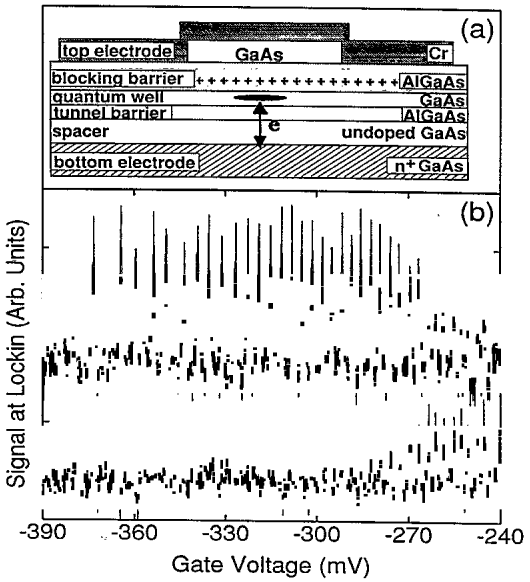

FIG. 1. (a) Schematic of sample. (b) Capacitance data vs gate bias for the quantum dot sample in zero magnetic field. The top and bottom traces show the signal resulting from electron tunneling in phase and electron tunneling in 90° lagging phase with the 210 kHz excitation voltage, respectively.

with a 1.5 μm diam metal disk. All measurements are taken at 0.35 K.

Figure 1(b) displays capacitance versus gate bias data for the quantum dot sample. The top trace is the signal observed in phase with the excitation voltage. A first peak appears at -373 mV and arises as the lowest electronic state of the dot becomes resonant with the Fermi energy of the n^+ electrode. With increasing positive gate bias subsequent electrons tunnel onto the quantum dot. Unlike our previous results in a larger dot, the peaks are spaced rather uniformly, with their separation decreasing slightly with increasing electron number. The constancy of the peak heights attests to the quantization of charge that is being moved onto the dot.

Beyond the 25th peak, the peak heights in the top trace of Fig. 1(b) drop due to a decrease in the tunneling rate. This interpretation is confirmed by measuring the signal at the dot in 90° lagging phase, shown in the bottom trace of Fig. 1(b), where peaks occur only for $N \geq 25$. This behavior is unambiguous evidence that the tunneling rate of electrons is becoming smaller than the 210 kHz excitation frequency. A slow tunneling rate causes an electron to "wait" a length of time before it tunnels in response to the excitation voltage, and its motion thus lags the excitation. Measurements on several wafers suggest that the decreasing rate is attributable to the thick 600 Å spacer layer, which itself acts as a long and low (< 20 meV) tunnel barrier.

The regime of a few electrons in a dot has been probed by relatively few experiments [5]. We now use SECS in the B field to study this domain with unprecedented resolution. Figure 2 is a color scale image of the dot capacitance as a function of gate bias and the B field applied perpendicular to the plane of the dot. The white, red, and black regions correspond to the highest, intermediate, and lowest capacitance, respectively. The gate bias scale is converted to an energy scale [1] by division by a lever arm of 2.0 ± 0.1 for this structure.

Figure 2 represents the B-field evolution of the first 35 N-electron g.s. energies of the quantum dot. The field dependence of the lowest energy state in Fig. 2(a) is smooth and is well described by the first electron in a cylindrically symmetric parabolic potential [6] $\frac{1}{2} m^* \omega_0^2 r^2$ with $\hbar\omega_0 = 5.4$ meV. The high field asymptote of this curve follows the dashed line in Fig. 2(a) with slope $\hbar\omega_c/2$. From the classical turning points of the lowest bound state we deduce a dot diameter of 408 Å.

In contrast to the first electron, the evolution of the ground state energy of two electrons shows a pronounced "bump" and a change of slope at about 1.5 T (see dot on second electron). We interpret this feature as a singlet-triplet crossing. Considering noninteracting states, the first two electrons in the dot fall into a twofold (spin) degenerate ground state for $B = 0$. At higher field, the energy difference between the ground orbital state and the first excited state shrinks, and the Zeeman effect causes a level crossing at 25 T for $\hbar\omega_0 = 5.4$ meV.

Electron-electron interactions significantly reduce the B field for this singlet-triplet crossing. Wagner, Merkt, and Chaplik [7] have calculated its position for parabolic quantum dots. For $\hbar\omega_0 = 5.4$ meV, the crossing is expected at 3.6 T, about a factor of 2 higher than seen in Fig. 2(a). The discrepancy may arise from the assumption of a strictly parabolic potential in the calculation. Such a singlet-triplet crossing has not been observed in atomic physics experiments due to the exceedingly high B field required (4×10^5 T for He). The weak binding of electrons in our quantum dot along with the small electronic mass shifts it to attainable fields.

The singlet-triplet crossing should exist *even in the absence* of a Zeeman splitting, arising solely from the electron-electron interaction [7]. The angular momentum quantum number m of the two electrons in the ground state increases with B, being equal to zero only at low field [7,8]. The energy difference between single-particle states of progressively larger angular momenta decreases with increasing B; in higher fields, it becomes advantageous for the system to place electrons in states of successively higher angular momenta (larger orbit radii) in order to decrease the Coulomb repulsion between electrons. To maintain exchange antisymmetry of the two-electron wave function, the system undergoes singlet-triplet (triplet-singlet) crossings as m switches from even (odd) to odd (even) numbers.

The Zeeman energy moves the first singlet-triplet crossing to yet lower fields. Moreover, at higher fields the Zeeman effect may force the system to remain in a spin triplet, allowing only transitions between odd m states. For our GaAs dot, the nature of transitions beyond the initial singlet-triplet crossing depends sensitively on the value of $\hbar\omega_0$ for the dot as well as on the precise shape of the bare confining potential. These transitions cause smaller changes of slope in the two-electron g.s. energy, and we do not attempt to label them here.

The data of Fig. 2(a) display several unexpected features. The bump seen in the g.s. energy of the two-electron system seems to progress through the few-electron system (white dots). Its position shifts monotonically to higher fields with increasing N, producing a clear "ripple" through the data set. It seems likely that these features are also spin related. Finally, selected traces of Fig. 2(a) show a distinct intensity loss with increasing B resulting from an unexplained decreased tunneling rate.

Figure 2(b) shows the ground state energies of the dot for $N = 6$–35 on an expanded field scale. In order to interpret the general features of this data set, we turn first to Fig. 3(a). This graph reproduces the highly intertwined single-particle states of a cylindrically symmetric parabolic potential with $\hbar\omega_0 = 1.12$ meV in a B field. N electrons in this system fill the N lowest energy states. The g.s. energy of the Nth electron should thus oscillate as levels cross as indicated in bold red for the fourteenth electron g.s. The oscillations cease at about 2 T. The density of electrons at the center of the dot is larger than

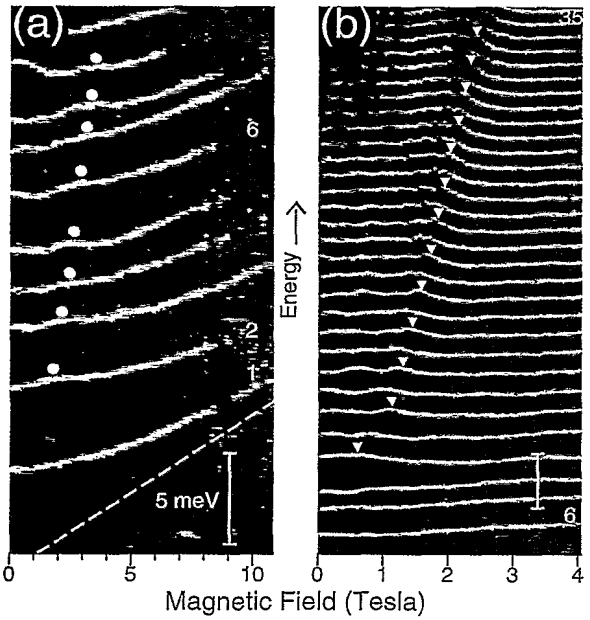

FIG. 2. Color scale plots of the sample capacitance as a function of both magnetic field and gate bias. The vertical bars in both (a) and (b) represent an energy of 5 meV. The dashed line shows $\hbar\omega_c/2$. Numerals along the traces indicate the electron number N. The magnetic field and energy scales are different in both (a) and (b). The symbols are discussed in the text.

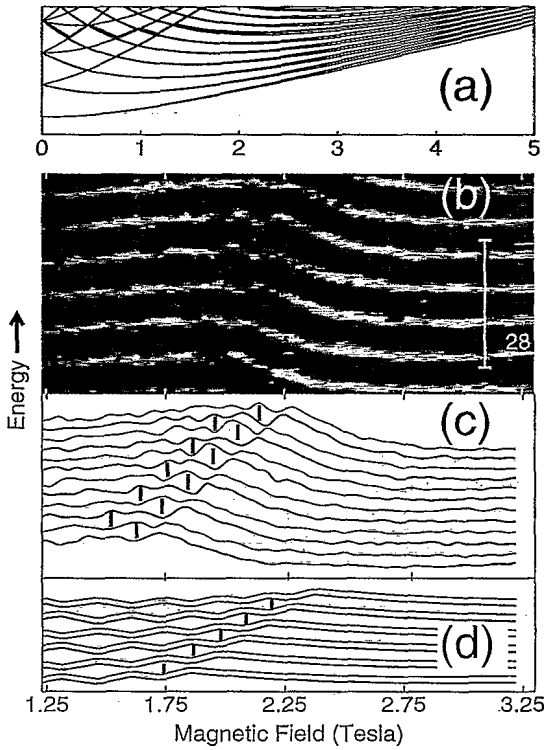

FIG. 3. (a) Theoretical Darwin-Fock states for a parabolic quantum dot with $\hbar\omega_0=1.12$ meV. The bold red curve displays the magnetic field evolution of the fourteenth electron. (b) Color scale capacitance data for $N=27$–32. (c) Measured N-electron ground state energies as a function of magnetic field for $N=21$–32, extracted from the data set which includes (b). (d) Evolution of N-electron ground states for $N=21$–32, calculated from the single-particle model. The vertical bar in (b) represents 5 meV and applies to all four windows.

at the dot's edges. Taking the Landau level index ν for the dot to be given by the Landau level occupancy at the dot center, the position of the last crossing in Fig. 3(a) can thus be identified with $\nu=2$, with two electrons at dot center per flux quantum passing through the dot.

In order to incorporate the electron-electron interaction to lowest order into this picture, we follow the constant interaction (CI) model [2,9,10]. It consists of single-particle states each separated by a charging energy, similar to what is shown in Fig. 3(d) and observed in Fig. 2(b). In Fig. 2(b), the development of the $\nu=2$ positions are clearly visible (white triangles). Beyond $N=10$, the $\nu=2$ positions for each successive electron agree well with the CI model using a constant $\hbar\omega_0=1.1$ meV. Curiously, the tunneling rates are attenuated around $\nu=2$ at large N. At $\nu=2$, the electrons in the dot center are in a quantum Hall state, and we speculate that tunneling suppression arises from the incompressibility of this state.

Figure 3(b), taken at 125 kHz, zooms in on the $\nu=2$ region for $N=27$–32. The oscillations expected from the CI model are clearly visible. To follow the traces more carefully, we fitted each capacitance peak of the original data set and plot their central positions in Fig. 3(c) for $N=21$–33. The traces have been moved together in the vertical direction for clarity. For comparison, Fig. 3(d) shows the results of the CI model for the same N values in a parabolic dot with $\hbar\omega_0=1.12$ meV using an arbitrary charging energy of 0.6 meV to separate the traces.

Although the qualitative agreement between experiment and the simple model is satisfying, there exist some remarkable differences. The CI model of Fig. 3(d) presents a pattern of oscillations with nearly uniform period and amplitude in each of the traces. The experi-

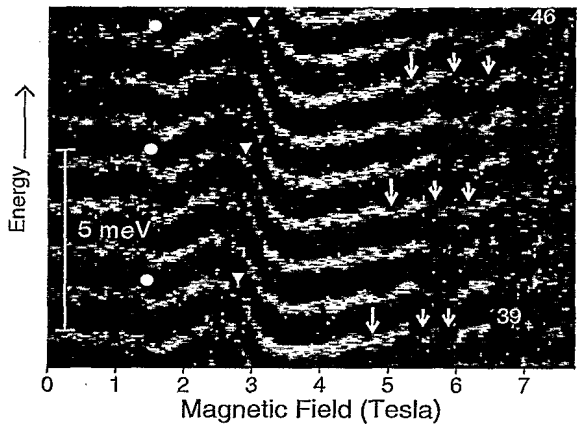

FIG. 4. Sample capacitance as a function of gate bias and magnetic field for $N=39$–46. The vertical bar represents an energy of 5 meV. The white symbols are discussed in the text.

mental traces of Fig. 3(c), on the other hand, show such oscillations only near $\nu=2$ and drop considerably for higher fields. In the CI model, we expect [Fig. 3(d)] that the g.s. energies for successive N-electron states will alternately oscillate in phase (due to spin degeneracy) and 180° out of phase. In the experiment [Fig. 3(c)] different pairs of successive traces display 180° phase shifts depending on the B-field value [red and blue bars in Fig. 3(c)]. While we presently have no explanation for the existence of oscillations only close to the $\nu=2$ region and their relative phases, we believe that the energy drop beyond $\nu=2$ is related to the nonparabolicity of the self-consistent potential.

Hartree calculations [11] show that the bottom of the dot's confinement potential is "flattened" considerably by the presence of electrons, and in the interior can be considered as a small two-dimensional (2D) system. In a 2D system there exist well-known sudden drops in the chemical potential as Landau levels depopulate in the B field. As N is increased, the dot approaches a 2D system, giving rise to the enhanced chemical potential drop at $\nu=2$ seen in our data.

The identification of the $\nu=2$ position allows us to determine the size of the dot, calculate its charging energy, and compare it with the observed gate bias spacing between successive electrons [9]. Since for large N the potential around the dot center is approximately constant, we can define a capacitance C of the dot to the electrodes. Ignoring the comparably small quantum level spacings, successive electron additions occur when the electrostatic potential in the dot changes by e/C. In a dot with a flat-bottom potential, the area of the dot A is related to the Landau level filling fraction ν by $A=N(h/eB\nu)$. For the 30th electron, $\nu=2$ occurs at about 2.2 T, which translates into a dot diameter of 1900 Å. Assuming parabolic confinement with $\hbar\omega_0=1.1$ meV rather than flat-bottom confinement decreases the dot area by only 2%. A simple parallel plate capacitor model neglecting fringing fields suggests peaks spaced 4.2 mV apart in gate bias, only ~25% larger than the measured spacing.

As we move to yet higher N, approaching the 2D limit, additional features become apparent in our spectra. Figure 4, taken at 125 kHz, displays the chemical potentials of the dot containing 39–46 electrons. Similar to Fig. 3(b), we observe the steep drop in chemical potential at B fields just beyond $\nu=2$ (white triangles). The same behavior is now apparent at $\nu=4$ (white dots). We attribute the accentuation of these features to the increasingly 2D character of the system at high filling.

Pursuing further the transition between a quantum dot and a finite-sized 2D electron system, we now examine the region $\nu<2$ at B above 4 T. We observe a sequence of "bumps" shifting only slightly to higher B with higher N. These features are inexplicable in terms of any CI model which all predict that successive traces oscillate 180° out of phase [2,10]. We hypothesize that the bumps seen in Fig. 4 are of many-particle origin reminiscent of the fractional quantum Hall effect (FQHE). In the FQHE the chemical potential of the system undergoes maxima between FQHE steps and minima at the steps [12]. The features seen in Fig. 4 are 0.2–0.5 meV in height, not unlike the characteristic energy range of the FQHE at such B fields. Moreover, the decrease in tunneling rates (intensity) between the bumps (see arrows in Fig. 4) may reflect the energy gaps in the FQHE. These features grow monotonically in prominence as more electrons are added to the dot, suggesting a two-dimensional origin. The size and distribution of the electron density within the dot vary with the B field, and it is thus difficult to assign a precise value of ν at dot center for fields beyond $\nu=2$. While the nonuniform electron density in the dot complicates the problem, one still expects FQHE minima [13] when the central portion of the dot is at a ν value appropriate for the FQHE.

We thank S. J. Pearton for help preparing the quantum dots and L. I. Glazman, P. Hawrylak, P. A. Lee, A. H. MacDonald, B. I. Shklovskii, and N. Wingreen for helpful discussions.

*Present address: Department of Physics, Massachusetts Institute of Technology, Cambridge, MA 02139.

[1] R. C. Ashoori, H. L. Stormer, J. S. Weiner, L. N. Pfeiffer, K. W. Baldwin, and K. W. West, Phys. Rev. Lett. **68**, 3088 (1992).

[2] P. L. McEuen, E. B. Foxman, U. Meirav, M. A. Kastner, Yigal Meir, Ned S. Wingreen, and S. J. Wind, Phys. Rev. Lett. **66**, 1926 (1991).

[3] Garnett W. Bryant, Phys. Rev. Lett. **59**, 1140 (1987).

[4] U. Meirav, M. Heiblum, and Frank Stern, Appl. Phys. Lett. **52**, 1268 (1988).

[5] B. Meurer, D. Heitmann, and K. Ploog, Phys. Rev. Lett. **68**, 1371 (1992); Bo Su, V. J. Goldman, and J. E. Cunningham, Science **255**, 313 (1992).

[6] C. G. Darwin, Proc. Cambridge Philos. Soc. **27**, 86 (1930).

[7] M. Wagner, U. Merkt, and A. V. Chaplik, Phys. Rev. B **45**, 1951 (1992).

[8] P. A. Maksym and Tapash Chakraborty, Phys. Rev. Lett. **65**, 108 (1990).

[9] R. H. Silsbee and R. C. Ashoori, Phys. Rev. Lett. **64**, 1991 (1990).

[10] P. L. McEuen, E. B. Foxman, Jari Kinaret, U. Meirav, M. A. Kastner, Ned S. Wingreen, and S. J. Wind, Phys. Rev. B **45**, 11419 (1992).

[11] Arvind Kumar, Steven E. Laux, and Frank Stern, Phys. Rev. B **42**, 5166 (1990).

[12] T. Chakraborty and P. Pietiläinen, *The Fractional Quantum Hall Effect* (Springer-Verlag, Berlin, 1988).

[13] Jari M. Kinaret, Yigal Meir, Ned S. Wingreen, Patrick A. Lee, and Xiao-Gang Wen, Phys. Rev. B **45**, 9489 (1992); A. H. MacDonald and M. D. Johnson, Phys. Rev. Lett. **70**, 3107 (1993).